Ceramics International **23** (1997) 93–98
© 1996 Elsevier Science Limited and Techna S.r.l.
Printed in Great Britain. All rights reserved
0272-8842(95)00144-1
0272-8842/97 $17.00+.00

Review Paper

Theoretical Aspects of Colloidal Processing

Yoshihiro Hirata

Department of Applied Chemistry and Chemical Engineering, Kagoshima University, 1-21-40 Korimoto, Kagoshima 890, Japan

(Received 10 September 1995; accepted 11 October 1995)

Abstract: Colloidal processing, which is composed of the dispersion of starting powders in liquid media and following consolidation, is superior to general dry pressing in the control of densities and microstructures of green and sintered compacts. The dispersion characteristic of the nanometre to submicrometre-sized powders in aqueous suspensions is greatly dominated by van der Waals attraction force and electrostatic repulsive force between colloidal particles. The critical solid content for highly viscous colloidal liquid, which was determined from the analysis of rheological properties, and increase of packing density during drying were compared with calculated metastable phase diagrams for one-component colloidal systems. The theoretical analysis on the pore structure in a powder compact was made with an fcc model (face-centred cubic close-packing) of hierarchically clustered spherical particles. The derived theory can reveal the pore volume and pore size distribution of 1st generation pores (contained within clusters of primary particles) and 2nd or 3rd generation pores (contained among the 1st or 2nd generation particle clusters). © 1996 Elsevier Science Limited and Techna S.r.l.

1 INTRODUCTION

Advanced ceramics are used in many fields, such as electronic, magnetic, optical, super-hard, high temperature structural, and biomaterials application. Many of the above ceramic materials are made from high purity submicrometre size powders. Since the function of ceramic materials depends on microstructure, "processing" to final materials through starting powders is very important in controlling the properties. Colloidal processing, which is composed of the dispersion of starting powders in liquid media and following consolidation, is superior to conventional dry pressing in the control of density and microstructure of green and sintered compacts.[1–5] Stability of a colloidal suspension is reflected in the property of a green compact, which in turn affects the property of a sintered material. Thus, the main purposes of colloidal dispersion and consolidation techniques are to control the packing density fluctuation in a green compact and the structure of hierarchically clustered particles during consolidation. The dispersion characteristics of a submicrometre size powder in an aqueous suspension is greatly dominated by the interaction energy based on the summation of van der Waals attraction force and electrostatic repulsive force between colloidal particles.[6] This article summarizes the key concept in controlling the density and structure of a powder compact by colloidal processing.

2 INTERACTION ENERGY BETWEEN COLLOIDAL PARTICLES

We consider the following four significant potential energies in colloidal systems of monosize spherical particles of the diameter D: Eg, gravity; Eb, buoyance; Ea, van der Waals attraction energy, and Er, repulsion energy by electric double layer. Equations (1) and (2) represent the potential energies Eg and Eb, respectively, for a spherical particle with the density ρ_s in a liquid medium with the density ρ_l,

$$E_g = \frac{\pi D^3}{6}\rho_s g h \tag{1}$$

$$E_b = -\frac{\pi D^3}{6}\rho_l g h \tag{2}$$

where g and h are the acceleration of gravity (9.807 ms^{-2}) and the height of the particle from the surface of the earth, respectively. The potential energy Ea is calculated by eqn (3),[7]

$$E_a = -\frac{A}{12}\left[\frac{D^2}{H^2+2DH} + \frac{D^2}{(H+D)^2} + \ln\frac{H^2+2DH}{(H+D)^2}\right] \tag{3}$$

where A and H are the Hamaker constant ($\sim 10^{-19}$J) and the distance between two particles,

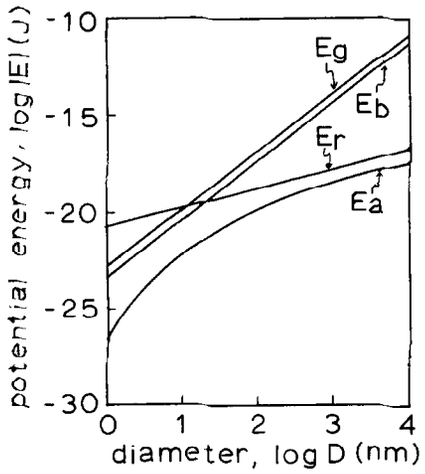

Fig. 1. Comparison of gravity (*Eg*), buoyance (*Eb*), van der Waals attraction energy (*Ea*) and repulsion energy by electric double layer (*Er*) for the colloidal system. See eqns (1)–(4) in the text for the calculation of potential energies.

respectively. Equation (4) corresponds to the potential energy *Er* between two charged particles,[7]

$$E_r = 32\pi\varepsilon\varepsilon_0 \frac{D}{2}\left(\frac{RT}{ZF}\right)^2 \tanh^2\left(\frac{ZF\phi}{4RT}\right)\ln[1+\exp(-\kappa H)] \quad (4)$$

ϵ: relative dielectric constant (78.3 for H2O), ε_0: permittivity of vacuum (8.854×10^{-12}F/m), R: gas constant (8.314J/mol · K), T: temperature (assumed to be 298 K), Z: charge number (assumed to be +1), F: Faraday constant (9.649×10^4 C/mol), ϕ: surface potential, $1/\kappa$: double layer thickness (assumed to be 10 nm).

Figure 1 illustrates the comparison of potential energies for the colloidal system under the conditions of h = 1 m, ρ_s = 3.2 gcm^{-3}, ρ_l = 1.0 gcm^{-3}, H = 10 nm and ϕ = 60 mV. All potential energies decrease with a decrease in particle size. The dominant potential energy changes from *Eg* to *Er* at a particle diameter of around 10 nm. Particle sedimentation effect caused by gravity can be neglected for fine particles smaller than about 10 nm. In powder processing of advanced ceramics, submicrometre size powders (100–1000 nm) are often used. Figure 1 suggests that submicrometre size particles in the aqueous colloidal suspension sediment finally and a phase separation (colloidal solid and medium liquid) occurs, resulting in the energetically most stable state of the colloidal system.[8,9] The properties of the colloidal suspensions before the phase separation are strongly influenced by the relative magnitude of the potential energies *Ea* and *Er*.

Figure 2 shows *Ea*, *Er* and summation *Ea* + *Er* for colloidal particles with diameters of 0.1 and 1.0 μm as a function of the distance H between two particles. Interaction energy between two charged particles (*Ei* = *Ea* + *Er*) gives the primary minimum

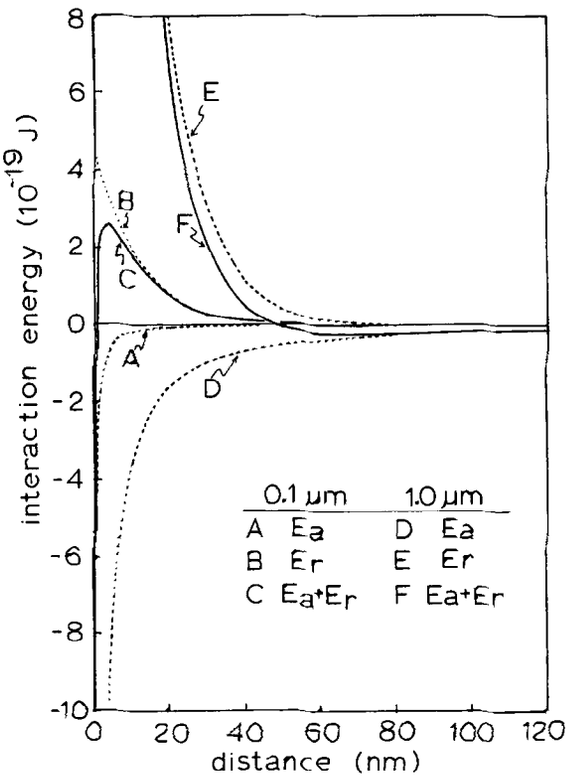

Fig. 2. Potential energies *Ea* and *Er*, and interaction energy (*Ea* + *Er*), for the colloidal system of particles of diameter 0.1 and 1.0 μm at ϕ = 60 mV as a function of distance between two particles.

(− ∞ at H = 0), primary maximum *Ei* (max) and secondary minimum *Ei* (min) as H is increased. As seen in Fig. 2, *Ei* (min) is very small compared with *Ei* (max) which becomes small with decreasing particle diameter. The energy difference between *Ei* (max) and *Ei* (min) corresponds to the activation energy for the formation of particle clusters from the dispersed state.

3 METASTABLE PHASE DIAGRAMS FOR COLLOIDAL SYSTEMS

Metastable phase diagrams illustrating the dispersion characteristics of colloidal particles were studied in the map of surface potential and solid content of the colloidal systems. Figure 3 shows simple cubic (SC) and hexagonal close-packing (HCP) models used in relating the interparticle distance H to the solid content X of a colloidal suspension. In these models, the following relations are derived,

$$X = k\left(\frac{D}{H+D}\right)^3 \quad (5)$$

where k is $\pi/6$ for SC model and $\sqrt{2}\pi/6$ for HCP model. Equation (5) indicates that a decrease in the distance H corresponds to an increase in solid content X.

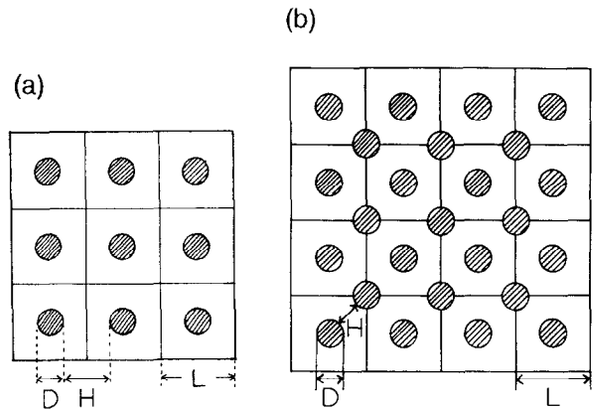

Fig. 3. Simple cubic (a) and hexagonal close-packing models (b) of lattice size L illustrating the structures of colloidal suspensions of spherical particles of diameter D.

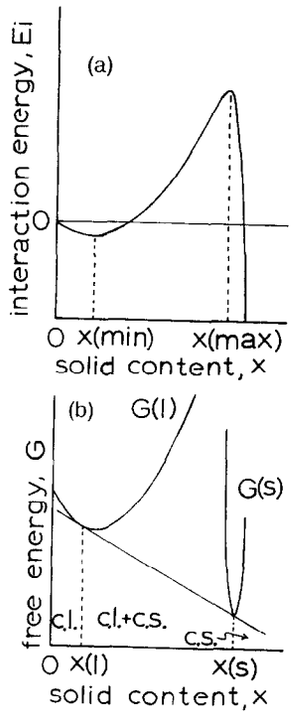

Fig. 4. Schematic illustrations of interaction energy (a) and free energy (b) as a function of solid content for one-component colloidal system. C.L. and C.S. mean colloidal liquid and colloidal solid, respectively.

Figure 4 illustrates schematically the solid content dependence on the interaction energy for the colloidal system.[8] The primary maximum is located at X(max) and the secondary minimum is located at X(min). The relation between interaction energy and phase transformation for the colloidal system can be understood more clearly by dividing the interaction energy into two parts which represent the natures of colloidal liquid and colloidal solid, as illustrated in Fig. 4. Interaction energy of colloidal particles is equivalent to Gibbs energy prescribing the thermodynamical stability of the colloidal system under the neglect of entropy term. The phases

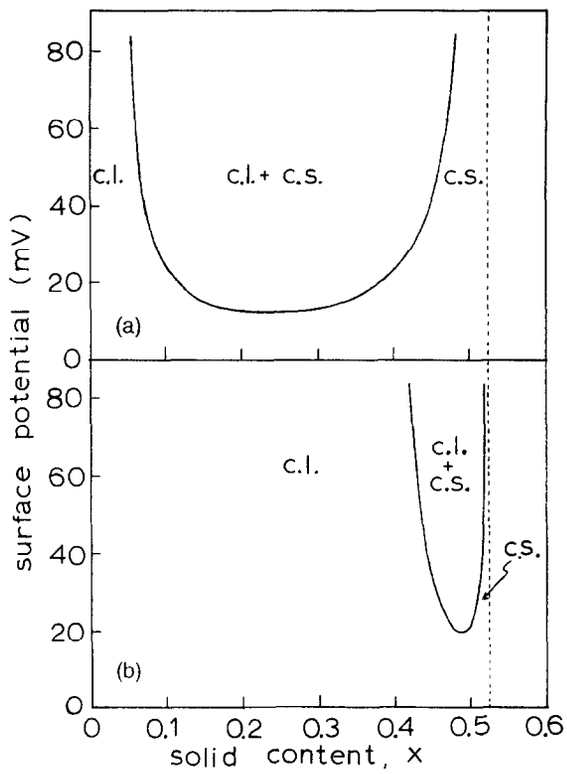

Fig. 5. Metastable phase diagrams for one-component colloidal systems of particles of diameters: (a) 0.1 μm and (b) 1.0 μm, based on a simple cubic model.

present in the colloidal system can be distinguished by a common tangent of free energies of colloidal liquid and colloidal solid. Solid content X(l) and X(s) would be approximated by X(min) and X(max), respectively.

Figure 5 summarizes the approximated solid contents X(l) and X(s) as a function of surface potential for particles of diameters 0.1 and 1.0 μm in a simple cubic model.[8] Similar phase diagrams were also calculated for HCP model. In colloidal systems, the interaction energy is easily varied by controlling the surface potential at room temperature, forming the same effect as changing T of phase diagrams for atomic systems. Figure 5 suggests that decreasing the particle size narrows the colloidal liquid range. That is, the colloidal system of smaller particles approaches the nature of colloidal solid at lower solid contents.[10] As the surface potential of particles approaches 0, the colloidal system behaves as a continuous body including complexed properties of colloidal liquid and colloidal solid.

4 RHEOLOGICAL PROPERTIES OF AQUEOUS SUSPENSIONS

The shear rate ($\dot{\gamma}$) versus shear stress (S) relation for suspensions of oxide powders of nanometre to

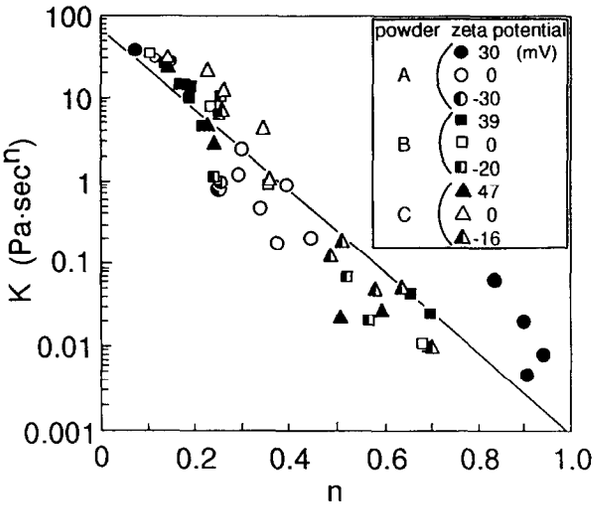

Fig. 6. Relation between n and K values in power law equation for the aqueous suspensions of mullite particles of 80 nm (powder A), alumina particles of 0.15 μm (powder B), and alumina particles of 0.35 μm (powder C).

submicrometre size was often described by an empirical power law equation (eqn (6), Ostwald–de Waale model),

$$S = K\dot{\gamma}^n \tag{6}$$

where K is the consistency index and n is the constant that indicates the departure from Newtonian behaviour.[11] The apparent viscosity (η_a) is expressed by eqn (7).

$$\eta_a = K\dot{\gamma}^{n-1} \tag{7}$$

The relation between n and K for mullite and alumina suspensions is summarized in Fig. 6, suggesting an empirical equation (8),

$$K = A\exp(-\beta n) \tag{8}$$

where A and β are the intercept at $n = 0$ and slope in Fig. 6.[12] The solid content at $n \to 0$ corresponds to one of a highly viscous colloidal solid giving a K value of 66.2 Pa (Fig. 6). The critical solid content (Vc) at $n \to 0$, estimated by extrapolating the apparent viscosity at $\dot{\gamma} = 9.6\ s^{-1}$ as a polynomial function of solid content to 6.9 Pa·s ($\eta_a = K/\dot{\gamma} = 66.2/9.6$ Pa·s).

The critical solid content of colloidal solid (Vc) and dried green compacts (Vg) as a function of zeta potential for oxide powders of 80 nm to 0.35 μm diameters are given in Fig. 7.[12] These data were compared with the metastable phase diagrams of one-component colloidal systems for 0.1 μm particles. The colloidal solid structure of submicrometer-sized powders is equivalent to the average structure of SC and HCP type colloidal solid (Fig. 7(b)). During drying or with increasing

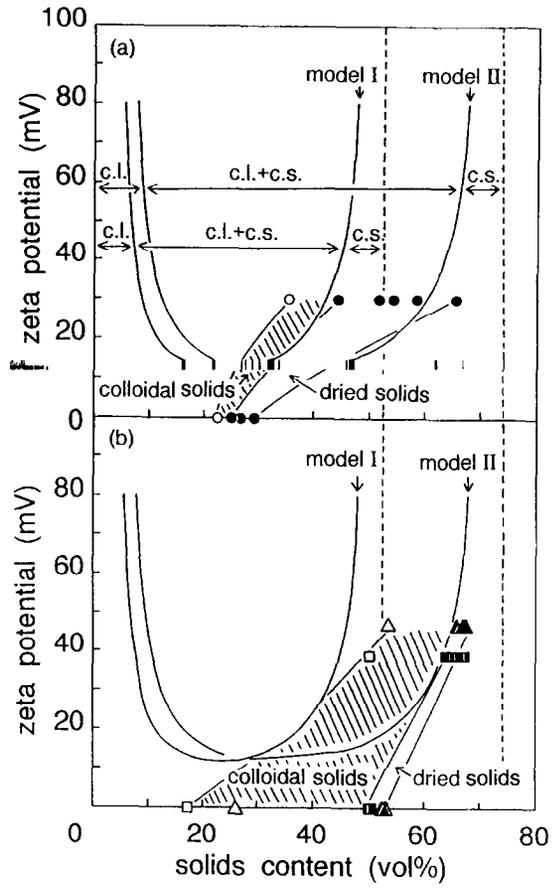

Fig. 7. Phase diagrams of colloidal systems based on (I) simple cubic model and (II) hexagonal close-packing model of spherical particles of 0.1 μm diameter and experimental data for (a) powder A and (b) powders B (□,■) and C (△,▲).

solid content of colloidal solid, the structures converge to the HCP type structure. Compared with submicrometre-sized powders, the colloidal solid range of the nanometre-sized powder (~80 nm) was narrow and close to the Vc curve of the SC model (Fig. 7(a)). The colloidal solid structure of nanometre-sized powder doesn't converge to a certain structure during drying. The low flexibility of colloidal solid structure, which was expressed by a narrow solid content range, leads to the freeze-drying type effect during drying, which results in a relatively wide density range of dried green compacts.[13]

5 PORE STRUCTURES OF POWDER COMPACTS

We consider a model structure shown in Fig. 8 for hierarchically clustered spherical particles. Since it was difficult to strictly analyse the continuous pore size distribution, we treated the pore structure as a set of three types of discrete pores of different sizes. Figure 9 summarizes green density and volume fraction of the 3rd generation pores (V(3p)) as a

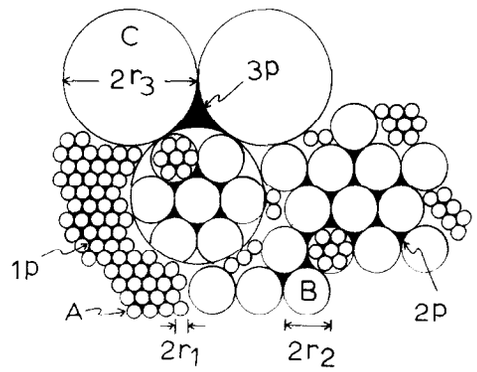

Fig. 8. A model structure of powder compact. A, B and C represent primary particle of diameter $2r_1$, 1st generation cluster of diameter $2r_2$ and 2nd generation cluster of diameter $2r_3$, respectively. Pores of 1p, 2p and 3p mean 1st, 2nd and 3rd generation pores formed among primary particles (A), 1st generation clusters (B) and 2nd generation clusters (C), respectively.

function of 2nd generation pore volume ($V(2p)$).[14] Points 1, 2 and 3 are made up in fcc of only primary particles, 2nd generation clusters and 1st generation clusters, respectively. Regions P and S illustrate the allowed pore region and corresponding solid content of the green compact. In our calculation, the volume fraction of 1st generation pores depends only upon the packing density of solid ($V(1p)) = 0.3504\ V(s)$). As seen in Fig. 9, several structures of the green compacts can be made up to a fixed green density. These types of pore distributions play an important role on the densification of a green compact.

In fcc structure, the diameter of spherical pores ($2r_p$) surrounded by 4 particles (or clusters) and 6 particles (or clusters) is related to the diameter of particle or cluster ($2r$) as follows.

$$2r_p(4 - \text{coordination}) = 0.2247 \cdot 2r \qquad (9)$$

$$2r_p(6 - \text{coordination}) = 0.4142 \cdot 2r \qquad (10)$$

Since the ratio for the number of 4- and 6-coordination space in fcc structure is 2:1, the relative pore volume was approximated to be 0.758 for 6-coordination pores and 0.242 for 4-coordination pores. Figure 10 shows the calculated pore size distributions of the powder compacts of densities 0.6 and 0.7 along the line from point 3 to point 1 in Fig. 9. The diameter of primary particle was assumed to be 0.1 μm. As shown in Fig. 10, reduction of the cluster size leads to (i) increase of the green density, (ii) increase of the volume of 1st generation pores, (iii) decrease of the volume of 2nd generation pores, and (iv) decrease of the pore size of 2nd generation pores.

Figure 11(a) illustrates the pore size distribution of mullite powder compact (particle diameter: 65 nm)

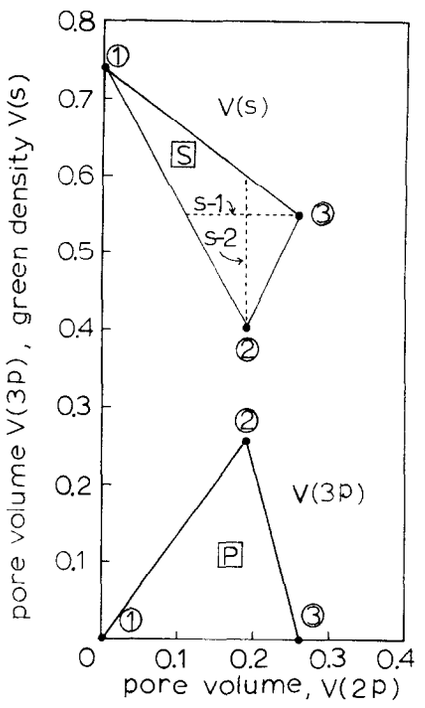

Fig. 9. Allowed pore region (P) and corresponding green density region (S) for the model structure of fcc in Fig. 8. V(2p), V(3p) and V(s) mean the volume fraction of 2nd generation pores, 3rd generation pores and green density, respectively.

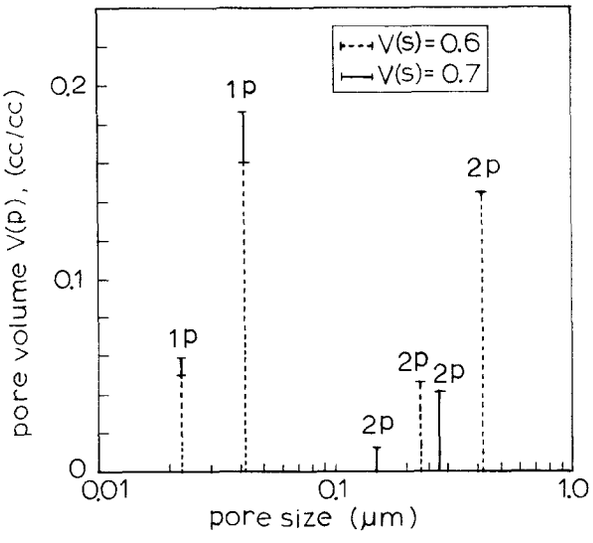

Fig. 10. Calculated pore size distributions of powder compacts of green densities 0.6 and 0.7 along the line from point 3 to 1 in Fig. 9.

with densities of 0.635. The theoretical lines express well the feature of measured pore size distribution, indicating no 3rd generation pores. Compared with Fig. 11(a), the pore structure in Fig. 11(b) becomes more complicated due to the formation of 2nd generation clusters and a wide agglomerate size distribution. However, the meaning of measured pore size distribution can be well understood by the theoretical prediction.

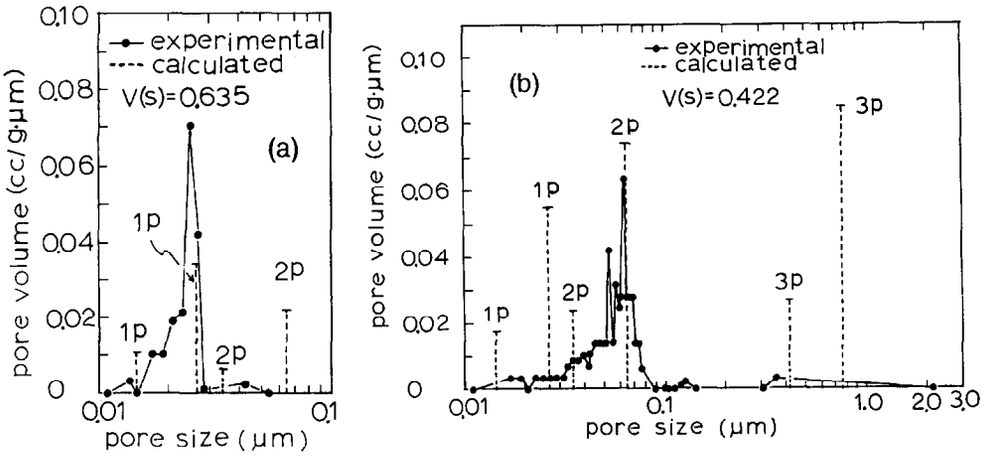

Fig. 11. Pore size distributions of mullite compacts of green density (a) 0.635 and (b) 0.422.

6 CONCLUSIONS

All potential energies (gravity, buoyancy, van der Waals attraction energy and repulsive energy by electric double layer) of an interacting colloidal spherical solid in an aqueous suspension decrease with decreasing particle size. In the particle size range below 100 nm, the potential energy of repulsion between charged particles with a typical surface potential of 60 mV becomes comparable with the energy by gravity. Metastable phase diagrams for one-component colloidal systems were constructed from the interaction energy curve between charged particles as a function of solid content. These phase diagrams suggest that (i) the nature of colloidal suspensions of smaller particles approaches colloidal solid at lower solid contents, and (ii) as the surface potential of particles approaches 0, it is difficult to identify the property of the colloidal system to be colloidal liquid or colloidal solid. Analysis of rheological properties of aqueous suspensions were compared with the above phase diagrams and led to the following conclusions. The colloidal structures of submicrometre-sized powders converge to a close-packing structure during drying with little dependence of green density on the concentration of colloidal suspension. In contrast, a nanometre-sized powder doesn't converge to a certain structure during drying due to the low flexibility of colloidal solid structure, indicating high solid concentration dependence of green density. Pore size of 1st generation pores formed among primary particles is independent of the green density, but the size and volume of higher hierarchical pores formed among particle clusters can be decreased by reducing the size of particle clusters. Consequently, reducing the degree of hierarchy of particle clusters leads to the achievement of a narrower pore size distribution of smaller average size and higher packing density.

REFERENCES

1. AKSAY, I. A., LANGE, F. F. & DAVIS, B. I., *J. Am. Ceram. Soc.*, **66** (1983) C–190.
2. LANGE, F. F., DAVIS, B. I. & WRIGHT, E., *J. Am. Ceram. Soc.*, **69** (1986) 66.
3. BLEIER, A. & WESTMORELAND, C. G., *J. Am. Ceram. Soc.*, **74** (1991) 3100.
4. LEE, H. & SACKS, M. D., *J. Am. Ceram. Soc.*, **73** (1990) 1884.
5. RUSSEL, W. B., *Mater. Res. Bull.*, **XVI** (1991) 27.
6. AKSAY, I. A., Fundamentals of powder consolidation in colloidal systems. In *Ceramics Today and Tomorrow*, ed. S. Naka, N. Soga & S. Kume. Ceramic Society of Japan, Tokyo, 1986, pp. 71–85.
7. SHAW, D. J., *Introduction to Colloidal and Surface Chemistry*. Butterworths Ltd, London, 1980, pp. 183–8.
8. HIRATA, Y., NAKAGAMA, S. & ISHIHARA, Y., *J. Ceram. Soc. Japan*, **98** (1990) 316.
9. AKSAY, I. A. & KIKUCHI, R., Structures of colloidal solids. In *Science of Ceramic Chemical Processing*, ed. L. L. Hench & D. R. Ulrich. John Wiley and Sons Inc., New York, 1986, pp. 513–21.
10. PUGH, R. J. & BERGSTROM, L., *Surface and Colloid Chemistry in Advanced Ceramic Processing*. Marcel Dekker Inc., New York, 1994, pp. 229–35.
11. KANNO, T., Rheological properties of raw materials for sintering. In *Evaluation Methods for Ceramics*. Ceramic Society of Japan, Tokyo, 1993, pp. 63–71.
12. HIRATA, Y., HARAGUCHI, I. & ISHIHARA, Y., *J. Mater. Res.*, **7** (1992) 2572.
13. HIRATA, Y., TAKESHIMA, K. & ISHIHARA, Y., *J. Ceram. Soc. Japan*, **100** (1992) 353.
14. HIRATA, Y., AKSAY, I. A. & KIKUCHI, R., *J. Ceram. Soc. Japan*, **98** (1990) 126.